Electrochemical Layer-by-Layer Growth of Palladium on an Au(111) Electrode Surface: Evidence for Important Role of Adsorbed Pd Complex

Hideo Naohara, Shen Ye, and Kohei Uosaki*

Physical Chemistry Laboratory, Division of Chemistry, Graduate School of Science, Hokkaido University, Sapporo 060-0810, Japan

Received: January 5, 1998; In Final Form: March 24, 1998

The adsorption and electrochemical reduction of the tetrachloropalladate complex, $PdCl_4^{2-}$, on an Au(111) electrode in H_2SO_4 solution containing $PdCl_4^{2-}$ was investigated using an electrochemical quartz crystal microbalance (EQCM) and in situ electrochemical scanning tunneling microscopy (STM). The adlayer of $PdCl_4^{2-}$ with a $(\sqrt{7} \times \sqrt{7})R19.1°$ structure on the Au(111) substrate was observed by in situ STM measurement, and the amount of adsorbed $PdCl_4^{2-}$ determined by the EQCM measurement was in good agreement with that estimated from this adlayer structure. In situ STM observation showed also that the electrochemical deposition of palladium proceeded with an epitaxial layer-by-layer growth mode and the $PdCl_4^{2-}$ complex adsorbed on the deposited palladium layer with the same adlayer structure. The adsorption of the $PdCl_4^{2-}$ complex seemed to play an important role for the layer-by-layer growth of palladium in a large area, since it inhibits the vertical but favors the lateral growth of the palladium layer. The formation of the Pd(111) bulk phase and the surface structure of Pd(111) was confirmed by X-ray diffraction (XRD) and the underpotential deposition of copper, respectively.

Introduction

Modifications of the properties of a solid surface by foreign atoms and molecules that are usually realized by physical vapor deposition in ultrahigh vacuum (UHV) or electrochemical plating in a electrolyte solution are very important not only in fundamental studies but also in industrial applications such as catalysis, electronics, and corrosion protection. In UHV, the epitaxial growth of a foreign metal layer on a substrate has been achieved by vapor deposition, molecular beam epitaxy (MBE). The structure of the epitaxial layer was analyzed by various methods in UHV, such as reflection high-energy electron diffraction (RHEED), low-energy electron diffraction (LEED), auger electron spectroscopy (AES), and X-ray photoelectron spectroscopy (XPS). The metal deposition by an electrochemical method in a solution containing a metal ion or metal complex should be more economical and convenient than the growth in UHV because the expensive UHV environment is not necessary. The structure of the electrodeposited metal layer is known to be controlled by many factors including deposition potential/current, concentration of metal ion/complex, nature of the additives, and surface structure of the substrate. To establish a method to electrochemically deposit a smooth epitaxial layer of foreign metals, it is essential to monitor the surface structure of the electrode during the electrochemical deposition process. The observation of the structure of the substrate and the metal adlayer with atomic resolution in an electrochemical environment is more difficult than that in UHV because of the existence of the electrolyte solution. Recently, in situ techniques for surface characterization in an electrolyte solution such as STM,[1] atomic force microscopy (AFM),[1−3] EQCM,[4] and surface X-ray scattering (SXS)[5,6] were applied for the investigation of the electrochemical deposition process. Although many reports are available for in situ observation of so-called underpotentially deposited (UPD) metal layers such as copper,[7] silver,[8] lead,[9] bismuth,[10] and tellurium,[11] the investigation of the electrochemical deposition process with atomic resolution is rather limited and only limited evidence has been provided for the adsorption of the reactant,[12−15] i.e., metal ions, on the electrode surface during the electrochemical deposition.

One of the most important metals for industrial applications and fundamental studies is palladium because of its high catalytic activities for many chemical reactions and ability to absorb hydrogen.[16] The growth of the ultrathin palladium layer on Au(111) prepared by vapor deposition in UHV was investigated by AES, LEED, and STM.[17−19] The results of the AES and LEED measurements showed that the palladium has grown on the Au(111) substrate in an epitaxial layer-by-layer mode for the first few layers at 150 K and that the surface alloy between the gold and palladium was formed at more than 500 K.[17,18] STM images showed, however, a rough morphology for the deposited palladium layer in which a simultaneous evolution of a number of layers was observed when 3.0 monolayers (ML) of palladium was dosed.[19] Recently, the epitaxial growth of a palladium layer on gold single-crystal electrodes by electrochemical deposition was confirmed by Baldauf and Kolb with in situ STM measurements.[20] The reaction rates of hydrogen adsorption and formic acid oxidation were investigated as a function of the thickness of the palladium layer on the gold substrate. A large difference between the palladium epitaxial thin layer and a bulk single crystal was observed,[20,21] suggesting an effect of the interaction with the substrate. However, the observation of electrochemical deposition of palladium with atomic resolution has not been carried out and the mechanism for the two-dimensional (2D) growth of palladium on gold is not clear yet.

In this paper, the adsorption of reactant, i.e., the $PdCl_4^{2-}$ complex, and the electrochemical deposition process of the

* Corresponding author. Telephone: +81-11-706-3812. Fax: +81-11-706-3440. E-mail: uosaki@PCL.sci.hokudai.ac.jp.

S1089-5647(98)00624-5 CCC: $15.00
Published on Web 05/07/1998

$PdCl_4^{2-}$ to palladium on an Au(111) electrode in H_2SO_4 solution containing $PdCl_4^{2-}$ are investigated by in situ electrochemical STM and EQCM measurements and the important role of the adsorbed $PdCl_4^{2-}$ species on the electrode surface for promoting the electrochemical 2D growth of the palladium layer is discussed.

Experimental Section

Materials. Electrochemical STM, electrochemical measurements, and XRD measurements were carried out at the surface of an Au(111) single crystal, which was prepared by Clavilier's method.[22] It was mechanically polished, annealed by a gas−oxygen flame for at least 4 h at ca. 800 °C and quenched in argon-saturated ultrapure water (Milli-Q, Millipore). For the EQCM measurements, the gold electrode was prepared by the vacuum evaporation of 10 nm of titanium followed by 150 nm of gold onto a 5 MHz AT-cut quartz crystal plate (double-side polished) at 300 °C with an evaporation rate of less than 0.01 nm/s. This procedure is known to provide a highly ordered Au(111) phase with wide terraces.[23] Before each measurement, the electrode was annealed by a gas−oxygen flame for a few seconds and then quenched in argon-saturated Milli-Q water.

Electrolyte solutions were prepared using H_2SO_4 (Suprapure reagent grade, Wako Pure Chemicals), $HClO_4$ (Suprapure reagent grade, Wako Pure Chemicals), K_2PdCl_4 (Reagent grade, Wako Pure Chemicals), $CuSO_4$ (Reagent grade, Wako Pure Chemicals), and Milli-Q water.

Electrochemical STM Measurements. In situ electrochemical STM measurements were carried out using a NanoScope E (Digital Instruments) control unit and a PicoSPM (Molecular Imaging) scanning unit with an airtight chamber and solution inlet tubes. STM images with atomic resolution were recorded as current images in a constant-height mode, and wide-range STM images were recorded as height images in a constant-current mode. A homemade electrochemical STM cell, which can accommodate a single-crystal electrode, was used. A small quasi-reversible hydrogen electrode and a platinum wire were used as the reference and the counter electrode, respectively. The electrolyte solution was deaerated by passing purified argon gas for at least 20 min before it was introduced into the STM cell. Electrochemical potentials of the Au(111) substrate (E_S) and STM tip (E_T) were independently controlled by a bipotentiostat (PicoSTAT, Molecular Imaging). STM tips were mechanically cut Pt/Ir wire (80/20, $\phi = 0.25$ mm) insulated with nail polish. Before each measurement, pure argon gas was passed to the STM chamber to purge the oxygen.

Electrochemical and EQCM Measurements. Electrochemical and EQCM measurements were carried out in a three-compartment cell with a Luggin capillary. The electrochemical potential was controlled by a potentiostat (HA-151, Hokuto Denko), and an external potential was provided by a function generator (HB-111, Hokuto Denko). A quasi-reversible hydrogen electrode and a platinum foil were used as the reference and the counter electrode, respectively. The potential is referenced to the reversible hydrogen electrode (RHE) in this paper. The resonant frequency of the quartz crystal electrode, which was oscillated by a homemade oscillation circuit, was simultaneously monitored with the electrode potential and current by a frequency counter (HP53131A, Hewlett-Packard) controlled by a personal computer (PC9821cb2, NEC) through a GPIB interface. The frequency stability of the EQCM system was better than 0.1 Hz for a sampling gate time of 0.1 s.

All the measurements were carried out after the solution was purged by passing pure argon gas for at least 20 min through the solution.

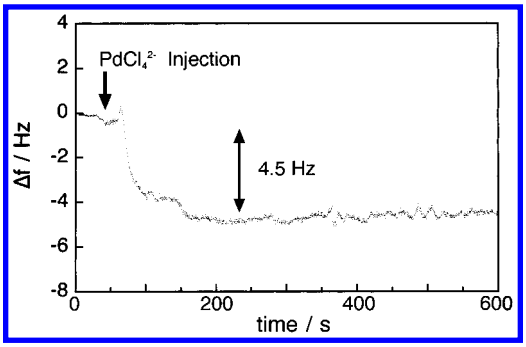

Figure 1. Time dependence of frequency change at +0.95 V when the $PdCl_4^{2-}$ solution was added to the EQCM cell that contained a 50 mM H_2SO_4 solution. The final concentration of $PdCl_4^{2-}$ in the cell was 0.1 mM.

The mass change (Δm) was calculated from the resonant frequency shift (Δf) using the Sauerbrey equation.[24] The mass sensitivity of the 5 MHz AT-cut quartz crystal was calibrated by the deposition of silver and lead.[13,25] Both measurements gave similar values, and −19.3 ng/Hz cm^2 was used for the calculation of the mass change.

XRD Measurements. The XRD measurement was carried out using a RINT-2200 (RIKAKU) with a four-circle diffractometer. After the electrochemical deposition of palladium on the Au(111) electrode, the electrode was moved from the electrolyte solution under potential control, then rinsed with Milli-Q water, and finally dried with purified argon gas. A palladium foil and the Au(111) single crystal were used for comparison.

Results and Discussion

Adsorption of $PdCl_4^{2-}$ Species on an Au(111) Electrode. Figure 1 shows the time dependence of frequency change at +0.95 V where neither a cathodic nor an anodic current was observed when 0.17 mL of 30.6 mM K_2PdCl_4 solution was added into the EQCM cell that contained 50 mL of 50 mM H_2SO_4 solution while the solution was stirred with a stirring bar. The final concentration of $PdCl_4^{2-}$ in the cell was 0.1 mM. The frequency was increased by 0.5 Hz in the first ca. 20 s of the induction period after the addition of $PdCl_4^{2-}$ and then abruptly decreased by 4.5 Hz, which corresponded to the surface mass increase of 86.9 ng/cm^2. The frequency did not change except for a little perturbation when the same volume of 50 mM H_2SO_4 solution was added to the EQCM cell. Thus, the mass increase should be related to the injection of the $PdCl_4^{2-}$ species. It is known, however, that the bisulfate anion is adsorbed on the Au(111) electrode surface at this potential.[26,27] A similar experiment was carried out in a 50 mM $HClO_4$ solution in which the ClO_4^- is considered as an unadsorbed species. The surface mass was changed in the same manner as the case in H_2SO_4 solution when the same amount of K_2PdCl_4 solution was introduced into $HClO_4$ solution. We therefore attributed the mass increase to the adsorption of $PdCl_4^{2-}$ on the Au(111) electrode surface. The number of adsorbed $PdCl_4^{2-}$ species calculated from the surface mass change was 2.1×10^{14}/cm^2, i.e., ca. 15% of that of the Au(111) surface atoms. This value was the same as that found for the adsorbed hexachloroplatinate complex, $PtCl_6^{2-}$, on Au(111) with the $(\sqrt{7} \times \sqrt{7})$-*R*19.1° structure that we recently reported.[13]

The structure of the $PdCl_4^{2-}$ adlayer was investigated by in situ electrochemical STM at +0.95 V in a 50 mM H_2SO_4 solution containing 0.05 mM $PdCl_4^{2-}$. The atomically ordered Au(111)−(1 × 1) structure (nearest-neighbor distance of ca.

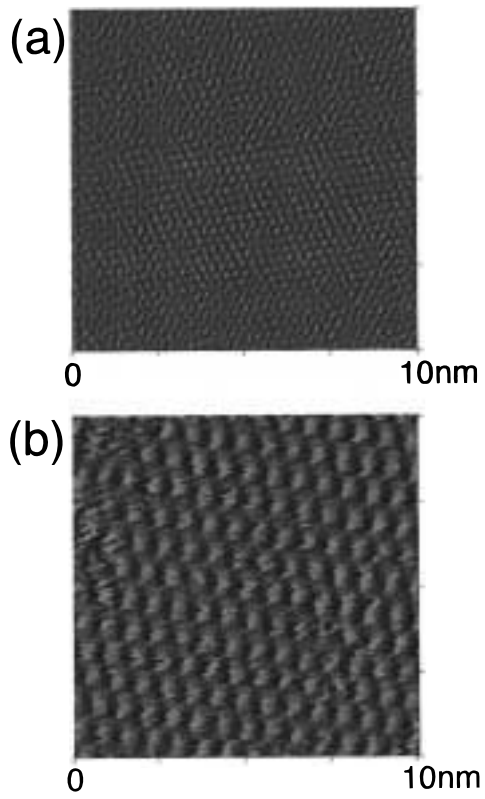

Figure 2. STM images (10×10 nm^2) of (a) an Au(111)$-(1 \times 1)$ electrode obtained at +0.95 V in a 50 mM H_2SO_4 solution and (b) the same electrode in a 50 mM H_2SO_4 solution containing 0.1 mM $PdCl_4^{2-}$ while the electrode potential was kept constant at +0.95 V.

0.29 nm) was observed at +0.95 V before the addition of $PdCl_4^{2-}$ (Figure 2a). When a 50 mM H_2SO_4 solution containing 0.1 mM $PdCl_4^{2-}$ was added into the electrochemical STM cell through the solution inlet tube which was attached to the airtight STM chamber (final concentration of $PdCl_4^{2-}$ of ca. 0.05 mM) while keeping the electrode potential at 0.95 V, a new structure of hexagonal symmetry with a nearest-neighbor distance of ca. 0.78 nm was observed (Figure 2b). The distance of 0.78 nm is $\sqrt{7}$ times that of the Au(111) lattice. The symmetry of the adlattice was found to be rotated by ca. 20° with that of the Au(111) substrate. This structure is different from that of a bisulfate adlayer, i.e., $(\sqrt{3} \times \sqrt{7})$ [26,28] but similar to that of the $PtCl_6^{2-}$ adlayer on Au(111).[13] Thus, we concluded that the $PdCl_4^{2-}$ complex was adsorbed on the Au(111) with the adlattice structure of $(\sqrt{7} \times \sqrt{7})R19.1°$. The number of adsorbed $PdCl_4^{2-}$ estimated from this structure is equal to 14% of that of the Au(111) surface atoms and is in very good agreement with that observed by EQCM measurements.

As the potential became more positive than +1.2 V, no clear STM image of the adlayer was obtained.

Electrochemical Deposition of Palladium. *EQCM Measurements*. After the adsorption of $PdCl_4^{2-}$ was completed in the H_2SO_4 solution at +0.95 V, the potential was scanned negatively to +0.35 V and then positively to +1.2 V. Simultaneously recorded current and mass changes during the potential sweep (5 mV/s) are shown in Figure 3 as a function of potential. A cathodic current started to flow as soon as the potential was made more negative than +0.95 V, reaching a maximum at +0.88 V and decreasing to a limiting value. The mass increase was observed at all the potentials during the cathodic scan from +0.95 to +0.35 V. The cathodic current observed in this region may be due to the reduction of gold oxide, the reduction of $PdCl_4^{2-}$ to palladium, or both.

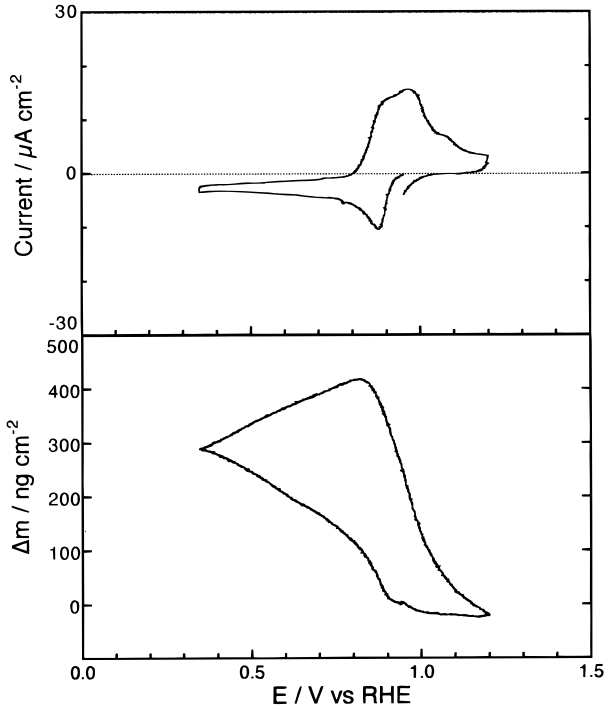

Figure 3. Potential dependence of (a) current and (b) mass change (Δm) at an Au(111) electrode in a 50 mM H_2SO_4 solution containing 0.1 mM $PdCl_4^{2-}$. Potential sweep rate was 5 mV s^{-1}.

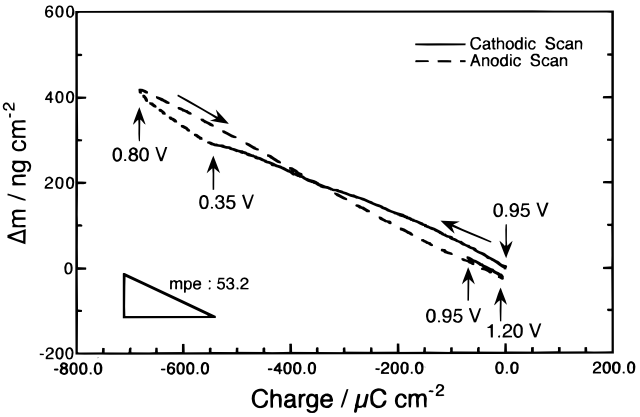

Figure 4. Relation between the mass change (Δm) and the charge (Q) obtained from Figure 3. The solid line and the dotted line represent the results obtained during the cathodic scan and the anodic scan, respectively.

To analyze the result more quantitatively, the mass change (Δm) was plotted against the charge, Q (solid line in Figure 4). A good linear relation was obtained in this potential region between +0.95 and +0.35 V during the cathodic scan. The slope of this plot gives the mass change per charge equivalent to one mole of electrons, mpe, as 51.3, which is in good agreement with the value expected for the following reduction process of the $PdCl_4^{2-}$ complex to palladium:[29]

$$PdCl_4^{2-} + 2e^- \rightarrow Pd + 4Cl^- \qquad (I)$$

If the preadsorbed palladium complex is reduced to palladium, the mass loss due to Cl^- desorption should be observed. Thus, the mass gain with an mpe of 51.3 means the reduction of the complex in the solution. Actually, the STM investigation described later showed that the palladium complex covered not only the gold substrate but also the deposited palladium surface during the deposition. Thus, the complex in solution seems to

be adsorbed on the surface as soon as the adsorbed complex is reduced and only the net mass change due to the Pd deposition was observed. The amount of the deposited palladium determined from the mass change from +0.95 to +0.35 V in this particular case was 1.2 monolayers (ML).

As the potential was swept in the anodic direction from +0.35 V, a relatively constant cathodic current flowed and the mass was uniformly increased to +0.80 V (Figure 3). The slope of Δm vs Q plot (broken line in Figure 4), mpe, in this region is close to the one observed during the cathodic scan, showing that the two-electron reduction of $PdCl_4^{2-}$ to palladium shown by eq 1 proceeded in this potential region. The mass increase reached a maximum value at +0.80 V, which was equivalent to a palladium deposition of 1.7 ML.

The anodic current started to flow at +0.80 V and increased as the potential became more positive, and two anodic peaks were observed at +0.89 and +0.96 V. A mass decrease was observed as soon as the anodic current started to flow. The anodic current observed at potentials more positive than +0.8 V could be due to the oxidation of palladium to palladium hydroxide,[30] the dissolution of palladium, or both. A very good linear relation in the Δm vs Q plot was obtained within this potential region (broken line in Figure 4) and the mpe was 63.4, which is in agreement with the value expected for the reverse reaction of reaction I, i.e., dissolution of palladium to the $PdCl_4^{2-}$ complex. If the (hydro-)oxide was formed, the surface mass should increase and mpe should be less than the above value. It is clear, therefore, that the observed anodic current was due to the dissolution of palladium. The amount of mass decrease in this potential region shows that all of the deposited palladium layer was dissolved.

During the negative potential sweep from +1.2 to +0.95 V, a small cathodic current flowed and the surface mass was slightly increased, showing the redeposition of palladium.

Figure 5a shows the time dependence of the current and the surface mass change simultaneously recorded in 50 mM H_2SO_4 solution containing 0.1 mM $PdCl_4^{2-}$ when the potential was stepped from +0.95 to +0.70 V. A sharp cathodic current spike was observed after the potential step and the surface mass gradually increased. A very good linear relation was obtained between the surface mass change and the charge calculated from the current in Figure 5a. The mpe calculated from the slope is 54.7, which is in very good agreement with the value expected for the two-electron reduction process given by eq I. It is interesting to note that an abrupt apparent surface mass increase of ca. 30 ng/cm^2, i.e., a frequency decrease of ca. 1.7 Hz, was observed around 190 s after the potential step. By this time, 290 ng/cm^2, i.e., one monolayer, of palladium was deposited. This abrupt change was observed in several independent experiments when the substrate was covered with ca. 1 ML of palladium. It is rather difficult to imagine that this change was due to the actual mass change. One possible explanation is the surface stress. It was reported that the resonance frequency of a quartz resonator was decreased when the surface stress was increased.[31] When the first monolayer of palladium was completed, the surface stress may increase, since there is a mismatch of 4% in the lattice spacing between gold and palladium.

In Situ STM Measurements. The deposition of $PdCl_4^{2-}$ was also investigated by in situ electrochemical STM. Figure 6 shows STM images (300 × 300 nm^2) of the Au(111) surface in a 50 mM H_2SO_4 solution containing 0.5 mM $PdCl_4^{2-}$. It took ca. 50 s to capture one image. Figure 6a is an STM image at +0.95 V where no palladium deposition takes place. A cross

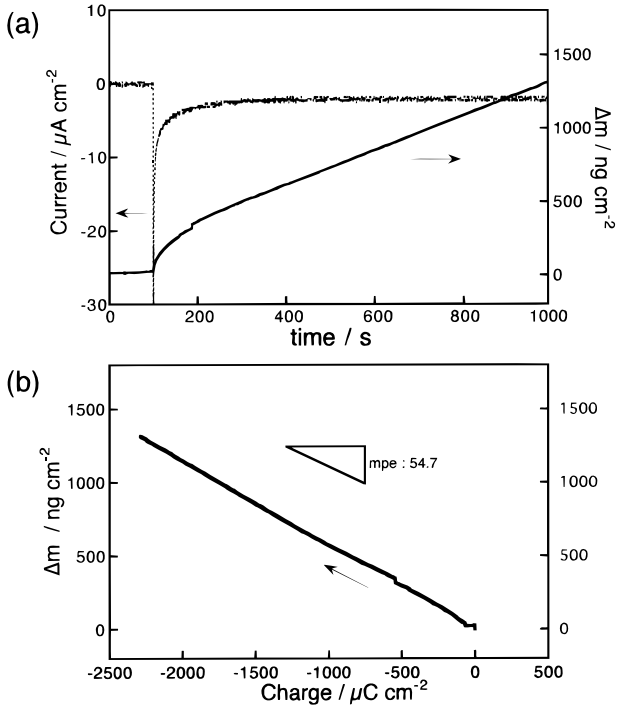

Figure 5. (a) Time dependence of current (dotted line) and the mass change (Δm, solid line) at an Au(111) electrode in a 50 mM H_2SO_4 solution containing 0.1 mM $PdCl_4^{2-}$ when the potential was stepped from +0.95 to +0.70 V. (b) Relationship between the mass change (Δm) and the charge (Q) after the potential was stepped from +0.95 to +0.75 V.

section along the white dotted line indicated in the STM image is shown as Figure 6a′. Atomically flat and large terraces (Terrace-1 and Terrace-2) and monatomic steps of gold of the Au(111) substrate were observed. Parts b−h of Figure 6 sequentially show obtained STM images of the same area (b) 0 min, (c) 1 min, (d) 2 min, (e) 3 min, (f) 28 min, (g) 48 min, and (h) 90 min after the electrochemical potential of the substrate (E_S) was stepped from +0.95 to +0.80 V as indicated by the thick arrow in Figure 6b where palladium deposition is expected to take place. The scan direction is shown by the arrow at the upper-left side of each figure. The electrochemical potential of the STM tip (E_T) was held at +1.0 V during the measurement. As soon as E_S was stepped from +0.95 to +0.80 V, the palladium nuclei were being generated on the Au(111) substrate. The cross section (Figure 6b′) along the dotted line shows the formation of the palladium islands with a monatomic height on the large terraces of the gold substrate. In the upper part of Figure 6b two-dimensional growth of the first palladium monolayer (Pd-1) progressed not only on the large terrace but also on a narrow terrace between the step lines. This result is in contrast to that observed by Baldauf and Kolb. They reported that the palladium layer started to preferentially grow from the step site.[20] This discrepancy should be due to the difference in the potential of the Au(111) substrate. As shown in parts c and c′ of Figure 6, after the first palladium layer (Pd-1) was completely formed on the gold substrate, islands of the second palladium layer (Pd-2) were generated on both Terrace-1 and Terrace-2 and the first palladium layer (Pd-1) on the narrow terrace started to grow laterally further onto the Pd-1 layer on Terrace-2 from the step line. Both the Pd-2 layer on Terrace-2 and the palladium layer extending from the Pd-1 layer on the narrow terrace grew two-dimensionally and merged, resulting in a large flat terrace of a second palladium layer on Terrace-2 (parts d and e of Figure 6). The cross section (parts c′, d′, and

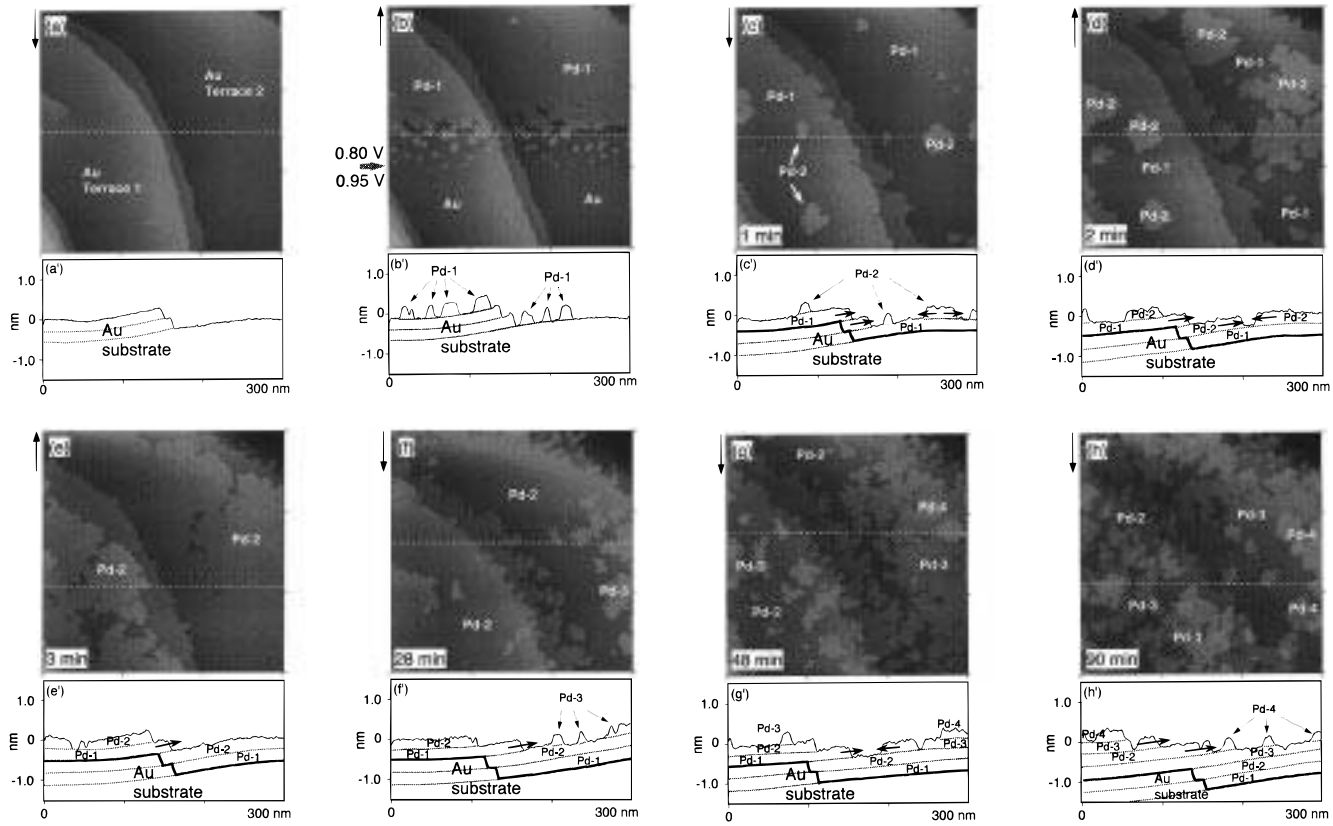

Figure 6. (a) STM image (300 × 300 nm^2) of an Au(111) substrate at +0.95 V in a 50 mM H_2SO_4 solution containing 0.5 mM $PdCl_4^{2-}$. Sequentially obtained STM images (300 × 300 nm^2) of the palladium deposition process on the Au(111) substrate (b) 0 min, (c) 1 min, (d) 2 min, (e) 3 min, (f) 28 min, (g) 48 min, and (g) 90 min after the potential were stepped from +0.95 to +0.80 V in the same solution. A cross section along with the white dotted line in each figure is shown below each image.

e′ of Figure 6) clearly shows the two-dimensional growth of the palladium monatomic layer. After the complete second palladium layer was formed on both Terrace-1 and Terrace-2, the third palladium layer (Pd-3) started to grow two-dimensionally on the terraces and from the step line (parts f and g of Figure 6). The growth rate of the third palladium layer was, however, slower than that of the first and the second layers. This should be due to the decrease in the local concentration of the reactant, i.e., $PdCl_4^{2-}$ near the surface, leading to a negative shift in the equilibrium potential for palladium deposition. The palladium layer, which was originally first deposited on Terrace 1, was also grown laterally and finally merged with Pd-3 on Terrace 2 (parts f−h of Figure 6).

Thus, palladium deposition proceeds in a layer-by-layer growth mode. Under these experimental conditions, an STM tip-induced local deposition, which we previously reported,[32] was not observed because E_T was more positive than E_S.

To investigate the deposition process more in detail, higher resolution images were obtained during the palladium deposition in 50 mM H_2SO_4 solution containing 0.5 mM $PdCl_4^{2-}$. Figure 7 shows the STM images (40 × 40 nm^2) (a) 20 s, (b) 40 s, and (c) 2 min after the potential was stepped from +0.95 to +0.87 V. In Figure 7a, monatomic-height palladium deposited layers are observed at the upper left and in the right region in the image. White spots are observed everywhere on the surface. Since the arrangement of these spots is the same as that of Figure 2b, these white spots should correspond to the adsorbed $PdCl_4^{2-}$ complex. Thus, the $PdCl_4^{2-}$ adsorbed not only on the gold substrate but also on the palladium layer with an ordered structure of $(\sqrt{7} \times \sqrt{7})R19.1°$. As time passed, palladium deposition proceeded two-dimensionally (Figure 7b) and the gold substrate was covered with the palladium, and finally an atomically flat palladium surface on which $PdCl_4^{2-}$ adsorbed with a $(\sqrt{7} \times \sqrt{7})R19.1°$ structure was obtained (Figure 7c). The second layer of palladium started to grow on top of the first palladium layer as observed at the right-bottom corners of parts b and c of Figure 7. .

The palladium layer grown electrochemically under the present conditions is very flat, and its domain is much larger than that of the vacuum-deposited palladium layer.[19] The adsorbed $PdCl_4^{2-}$ with a $(\sqrt{7} \times \sqrt{7})R19.1°$ structure on both the gold substrate and the deposited palladium layer should play a very important role in the present preferential 2D growth of the palladium layer.

Figure 8 shows a schematic model for the palladium deposition in the presence of the $PdCl_4^{2-}$ adlayer. The nucleation of palladium occurred at the surface defects. $PdCl_4^{2-}$ was also adsorbed on a deposited palladium island. The $PdCl_4^{2-}$ adlayer on the terrace of the palladium island should be more stable than that at the edge of the palladium island because of the interaction between the adsorbed species; therefore, the deposition rate of palladium on the terrace was greatly reduced. The deposition of palladium is easier at the edge site of an island where the blocking by $PdCl_4^{2-}$ is weaker than that on the terrace. Thus, the ordered $PdCl_4^{2-}$ adlayer inhibits the vertical but favors lateral, i.e., 2D, growth of the palladium layer as observed in the present experiment. A similar enhanced 2D growth of copper on an Au(111) electrode has been observed when organic additives are added to the solution.[7,33,34] The present result is, however, the first evidence for the effect of the adsorption of reactant itself, i.e., $PdCl_4^{2-}$, during the electrochemical dimension growth.

Characterization of Deposited Pd Layer. The structure of the deposited palladium layer was examined by means of X-ray

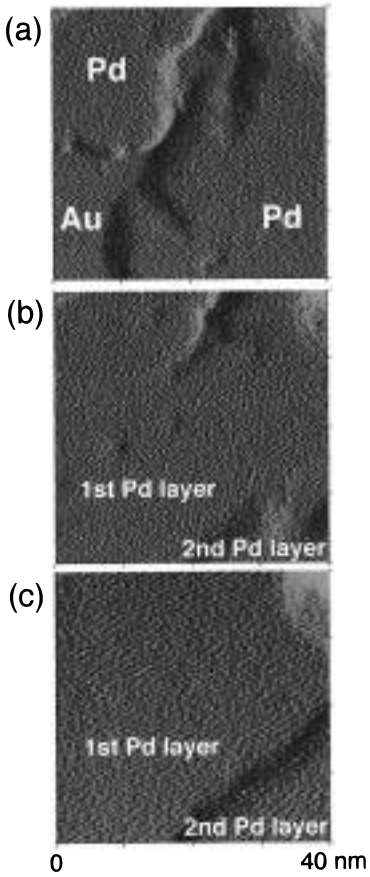

Figure 7. Sequentially obtained higher resolution STM images (40 × 40 nm^2) of the palladium deposition process on an Au(111) substrate (a) 20 s, (b) 40 s, and 2 min after the potential was stepped from +0.95 to +0.87 V in 50 mM H_2SO_4 solution containing 0.5 mM $PdCl_4^{2-}$.

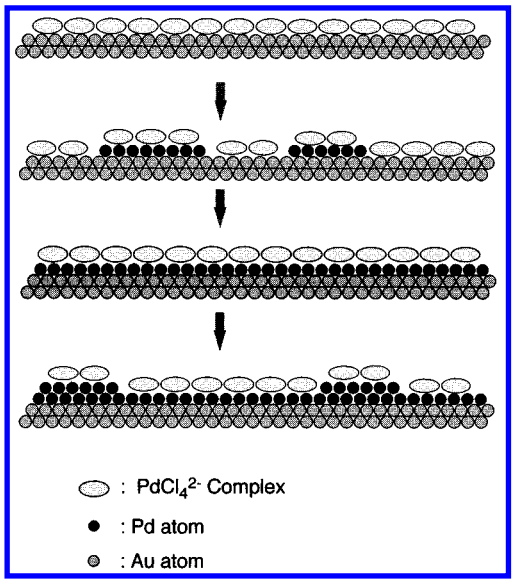

Figure 8. Schematic model for the palladium deposition process on an Au(111) substrate in the presence of the $PdCl_4^{2-}$ adlayer. The ordered $PdCl_4^{2-}$ adlayer inhibits the vertical but favors lateral, i.e., 2D, growth of the palladium layer as observed in the present experiment.

diffraction (XRD). Figure 9 shows the XRD patterns of (a) an Au(111) single crystal, (b) an Au(111) single crystal on which palladium was deposited electrochemically at 0.7 V for 1 h in a 50 mM H_2SO_4 solution containing 1 mM $PdCl_4^{2-}$ (Pd/Au-(111)), and (c) a bare polycrystalline Pd foil. The amount of the deposited palladium estimated from the charge was ca. 71

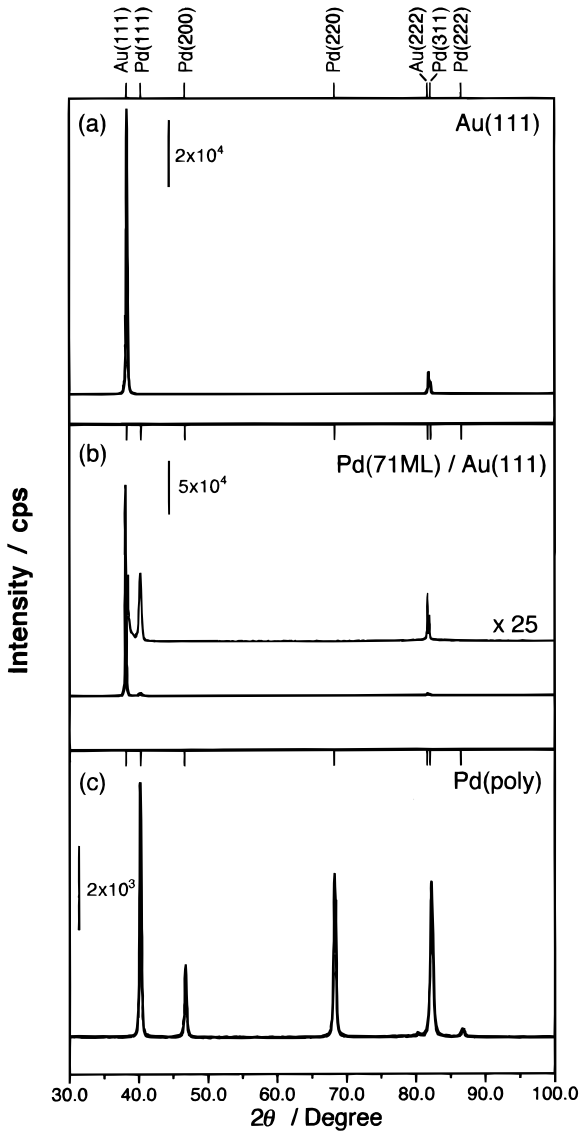

Figure 9. XRD patterns of (a) an Au(111) single-crystal electrode, (b) an Au(111) electrode followed by electrochemical deposition of palladium at 0.7 V for 1 h in a 50 mM H_2SO_4 solution containing 1 mM $PdCl_4^{2-}$ (amount of palladium deposited layer is equal to 71 ML) and (c) a polycrystalline Pd foil.

ML. The assignments based on the JCPDS data are given for the respective reflection peaks in the figure. For the Au(111) single crystal, only Au(111) and Au(222) peaks were observed. In addition to the Au(111) and Au(222) peaks, the (111) peak of palladium was observed in the XRD pattern of the Pd(71 ML)/Au(111) (Figure 9b). No other peaks due to palladium such as (200), (220), and (311), which were observed in the case of the polycrystalline palladium (Figure 9c), were observed. Thus, it is confirmed that the Pd(111) phase was deposited electrochemically on the Au(111) substrate.

The surface structure of the palladium deposited layer was also examined by recording the cyclic voltammograms (CVs) in H_2SO_4 solution and for the underpotential deposition (UPD) of copper (Figure 10). The shape of CV in general and the positions of the UPD peaks in particular of metal electrodes are known to be very sensitive to the surface structure and order.[7−11] After the deposition of palladium in 50 mM H_2SO_4 solution containing 0.01 mM $PdCl_4^{2-}$ at 0.7 V for 30 min (ca. 2 ML), the electrode was rinsed with milli-Q water. The CVs were recorded in another cell that contained a 50 mM H_2SO_4

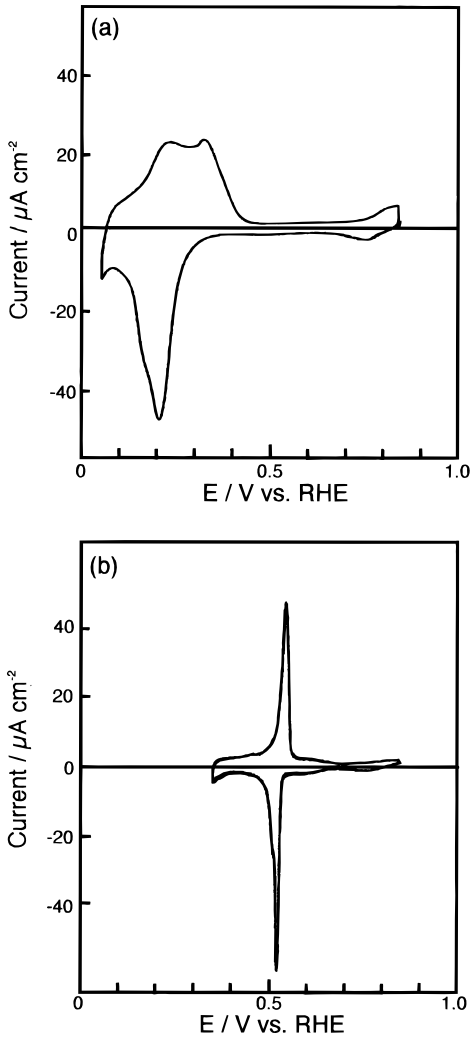

Figure 10. Cyclic voltammograms of the deposited palladium layer (ca. 2 ML) on an Au(111) electrode in (a) 50 mM H_2SO_4 solution (sweep rate of 50 mV s^{-1}) and (b) 5 mM $CuSO_4$ + 50 mM H_2SO_4 solution (sweep rate of 5 mV s^{-1}).

solution (Figure 10a) and a 50 mM H_2SO_4 + 5 mM Cu^{2+} solution (Figure 10b). The shape of the current−potential curve and the charge of hydrogen adsorption (214 μC cm^{-2}) on a Pd thin layer in a 50 mM H_2SO_4 solution were in good agreement with those reported by Baldauf et al.[20] Very sharp reduction and oxidation peaks with a full width at half-maximum (fwhm) of ca. 18 mV were observed in a 50 mM H_2SO_4 solution containing 5 mM Cu^{2+} at +0.52 and +0.54 V, respectively (Figure 10b). The copper stripping charge was 436 μC/cm^2. These values are close to those reported for copper UPD on a Pd(111) electrode in a 0.5 M $NaClO_4$ + 10^{-2} M $HClO_4$ + 10^{-3} M Cu^{2+} solution (sweep rate of 10 mV/s). The CV of copper UPD on a Pd(111) electrode shows a pair of very sharp redox peaks (+0.45 and +0.47 V, fwhm of 20 mV). The stripping charge was 440 μC/cm^2. The small difference in peak potentials reflects the difference in Cu^{2+} concentration. The CV of copper UPD in a polycrystalline palladium electrode is totally different from these CVs and shows three pairs of redox peaks (+0.26/+0.27, +0.46/+0.47, and +0.48/+0.49 V) in the same solution.[35] Furthermore, the potentials of the copper UPD peaks are completely different from those of copper UPD on an Au(111) electrode (+0.56/+0.57 and +0.38/+0.41 V). Thus, it was confirmed that the deposited palladium layer on the Au(111) electrode was the epitaxially grown Pd(111) phase. The alloy formation between gold and palladium, which was observed in UHV (>500 K),[17,18] did not take place under this condition.

Conclusion

The adsorption and electrochemical reduction of $PdCl_4^{2-}$ on an Au(111) electrode in a H_2SO_4 solution was investigated by EQCM and in situ electrochemical STM. The adlayer of $PdCl_4^{2-}$ with a $(\sqrt{7} \times \sqrt{7})R19.1°$ structure on an Au(111) substrate was observed by STM measurement, and the amount of the adsorbate determined by EQCM measurement was in good agreement with the values expected for this structure. Palladium deposition proceeded with an epitaxial layer-by-layer growth mode, and the adlayer of $PdCl_4^{2-}$ with a $(\sqrt{7} \times \sqrt{7})R19.1°$ structure was observed on the deposited palladium layer. The important role of the $PdCl_4^{2-}$ adlayer on the growth mechanism was suggested.

Acknowledgment. This work was partially supported by a Grant-in-Aid for Scientific Research on Priority Area of "Electrochemistry of Ordered Interfaces" (No. 09237101) from the Ministry of Education, Science, Sports and Culture, Japan.

References and Notes

(1) Gewirth, A. A.; Niece, B. K. *Chem. Rev.* **1997**, *97*, 1192.
(2) LaGraff, J. R.; Gewirth, A. A. *Nanoscale Probes of the Solid/Liquid Interface*; Gewirth, A. A., Siegenthaler, H., Eds.; Kluwer Academic Publishers: Dordrecht, 1995; pp 83−101.
(3) Uosaki, K.; Koinuma, M.; Sekine, N.; Ye, S. *Solid−Liquid Electrochemical Interfaces*; Jerkoiewicz, G., Soriaga, M. P., Uosaki, K., Wieckowski, A., Eds.; American Chemical Society: Washington, DC, 1997; pp 189−201.
(4) Buttry, D. A.; Ward, M. D. *Chem. Rev.* **1992**, *92*, 1355.
(5) Toney, M. F. *Synchrotron Techniques in Interfacial Electrochemistry*; Melendres, C. A., Tadjeddine, A., Eds.; Kluwer Academic Publishers: Dordrecht, 1994; pp 109−125.
(6) Ocko, B. M.; Wang, J. *Synchrotron Techniques in Interfacial Electrochemistry*; Melendres, C. A., Tadjeddine, A., Eds.; Kluwer Academic Publishers: Dordrecht, 1994; pp 127−155.
(7) Will, T.; Dietterle, M.; Kolb, D. M. *Nanoscale Probes of the Solid/Liquid Interface*; Gewirth, A. A., Siegenthaler, H., Eds.; Kluwer Academic Publishers: Dordrecht, 1995; pp 137−162.
(8) Ogaki, K.; Itaya, K. *Electrochim. Acta* **1995**, *40*, 1249.
(9) Tao, N. J.; Pan, J.; Li, Y.; Oden, P. I.; DeRose, J. A.; Lindsay, S. M. *Surf. Sci. Lett.* **1992**, *271*, L338.
(10) Chen, C.-h. C.; Gewirth, A. A. *J. Am. Chem. Soc.* **1992**, *97*, 9754.
(11) Ikemiya, N.; Iwai, D.; Yamada, K.; Vidu, R.; Hara, S. *Surf. Sci.* **1996**, *369*, 199.
(12) Sawaguchi, T.; Yamada, T.; Okinaka, Y.; Itaya, K. *J. Phys. Chem.* **1995**, *99*, 14149.
(13) Uosaki, K.; Ye, S.; Oda, Y.; Haba, T.; Hamada, K. *Langmuir* **1997**, *13*, 594.
(14) Uosaki, K.; Ye, S.; Naohara, H.; Oda, Y.; Haba, T.; Kondo, T. *J. Phys. Chem. B* **1997**, *101*, 7566.
(15) Haiss, W.; Sass, J.-K. *J. Electroanal. Chem.* **1997**, *431*, 15.
(16) Somorjai, G. A. *Introduction to Surface Chemistry and Catalysis*; John Wiley & Sons: New York, 1994.
(17) Koel, B. E.; Sellidj, A.; Paffett, M. T. *Phys. Rev. B* **1992**, *46*, 7846.
(18) Baddely, C. J.; Barnes, C. J.; Wander, A.; Ormerod, R. M.; King, D. A.; Lambert, R. M. *Surf. Sci.* **1994**, *314*, 1.
(19) Baddely, C. J.; Ormerod, R. M.; Stephenson, A. W.; Lambert, R. M. *J. Phys. Chem.* **1995**, *99*, 5146.
(20) Baldauf, M.; Kolb, D. M. *Electrochim. Acta* **1993**, *38*, 2145.
(21) Baldauf, M.; Kolb, D. M. *J. Phys. Chem.* **1996**, *100*, 11375.
(22) Clavilier, J. *J. Electroanal. Chem.* **1980**, *107*, 211; **1980**, *107*, 205.
(23) Uosaki, K.; Ye, S.; Kondo, T. *J. Phys. Chem.* **1996,** *99*, 1411.
(24) Sauerbrey, G. Z. *Z. Phys.* **1959**, *155*, 206.
(25) Bruckenstein, S.; Swathirajan, S. *Electrochim. Acta* **1985**, *30*, 851.
(26) Edens, G. J.; Gao, X.; Weaver, M. J. *J. Electroanal. Chem.* **1994**, *375*, 357.
(27) Shi, Z.; Lipkowski, J.; Gamboa, M.; Zelenay, P.; Wieckowski, A. *J. Electroanal. Chem.* **1994**, *366*, 317.
(28) Magnussen, O. M.; Hageböck, J.; Hotlos, J.; Behm, R. J. *Faraday Discuss.* **1992**, *94*, 329.

(29) Llopis, J. F.; Colom, F. *Encyclopedia of Electrochemistry of the Elements*; Bard, A. J., Ed.; Marcel Dekker: New York, 1976; Vol. VI.
(30) Kessler, T.; Visntin, A.; Bolzan, A. E.; Andreasen, G.; Salvarezza, R. C.; Triaca, W. E.; Arvia, A. J. *Langmuir* **1996**, *12*, 6587.
(31) EerNisse, E. P. *J. Appl. Phys.* **1972**, *43*, 1330.
(32) Naohara, H.; Ye, S.; Uosaki, K. *Appl. Phys. A*, in press.
(33) Nichols, R. J.; Bach, C. E.; Meyer, H. *Ber. Bunsen-Ges. Phys. Chem.* **1993**, *97*, 1012.
(34) Nichols, R. J. *Nanoscale Probes of the Solid/Liquid Interface*; Gewirth, A. A., Siegenthaler, H., Eds.; Kluwer Academic Publishers: Dordrecht, 1995; pp 163−182.
(35) Chierchie, T.; Mayer, C. *Electrochim. Acta* **1988**, *33*, 341.